

**PREMIXED FLAMELESS COMBUSTION OF  
PRODUCER GAS IN A CYCLONE COMBUSTOR**

**LEMTHONG CHANPHAVONG**

**UNIVERSITI SAINS MALAYSIA**

**2019**

# **PREMIXED FLAMELESS COMBUSTION OF PRODUCER GAS IN A CYCLONE COMBUSTOR**

by

**LEMTHONG CHANPHAVONG**

**Thesis submitted in fulfilment of the requirements  
for the degree of  
Doctor of Philosophy**

**September 2019**

## **ACKNOWLEDGEMENT**

Foremost, I would like to express the gratefulness to my supervisor, Professor Zainal Alimuddin Bin Zainal Alauddin, for his contributions of time, guidance, and encouragement during my study time. It was great opportunity to do the research under his supervision. Furthermore, I would like to thank Dr. Khaled for his guidance and advices for the experiment works as well as all technical staff at School of Mechanical Engineering, Universiti Sains Malaysia, for their time and technical supports.

I would like to acknowledge my co-supervisor, Professor Yuji Nakamura, Department of Mechanical Engineering, Toyohashi University of Technology (TUT), for his guidance and advice for the chemical kinetics modelling works and also extending my acknowledgement to all staff in his laboratory (Energy Conversion Engineering Laboratory) for assistance during my 8 months study in Japan.

Importantly, I am acknowledged AUN/SEED-net program under JICA project as well as both sending institution (National University of Laos -NUoL) and host institution (Universiti Sains Malaysia -USM) for supporting the scholarship for my doctoral study. I have met good friends and kindly staff at USM, especially at the School of Mechanical Engineering. I am grateful to them for their warmness and happiness during the past years while I was being studied here.

Lastly, I am grateful best appreciation to my family for invaluable support during my study.

## TABLE OF CONTENTS

<b>ACKNOWLEDGEMENT .....</b>	<b>ii</b>
<b>TABLE OF CONTENTS.....</b>	<b>iii</b>
<b>LIST OF TABLES .....</b>	<b>vii</b>
<b>LIST OF FIGURES .....</b>	<b>ix</b>
<b>LIST OF SYMBOLS .....</b>	<b>xvi</b>
<b>LIST OF ABBREVIATIONS .....</b>	<b>xx</b>
<b>ABSTRAK .....</b>	<b>xxii</b>
<b>ABSTRACT .....</b>	<b>xxiv</b>
<b>CHAPTER 1 INTRODUCTION.....</b>	<b>1</b>
1.1 Overview .....	1
1.2 Producer gas as an alternative gas fuel.....	2
1.3 Flameless combustion as a promising combustion for PG fuel .....	4
1.3.1 Definition of flameless combustion .....	4
1.3.2 Benefits and application status of flameless combustion.....	6
1.4 Problem statement .....	8
1.5 Objective of study .....	9
1.6 Scope and limitation.....	10
1.7 Thesis outline .....	11
<b>CHAPTER 2 LITERATURE REVIEW.....</b>	<b>12</b>
2.1 Improvement of combustion performance .....	12
2.1.1 Determination of flameless combustion region .....	13
2.1.2 Determination of reaction regime under flameless combustion .....	15
2.2 Development of PG combustion technology .....	17
2.2.1 PG combustion parameters with burner application .....	17
2.2.2 Combustion stabilization with swirl vane and bluff-body .....	21

2.2.3	PG combustion in staged combustor.....	24
2.2.4	PG combustion in swirl flow combustor.....	26
2.3	PG combustion under flameless combustion .....	29
2.3.1	Simulated PG mixture application .....	29
2.3.2	Actual PG mixture application.....	33
2.3.3	PG combustion in porous media burner.....	35
2.4	Other low heating value fuels with flameless combustion.....	37
2.5	Premixed and swirl flow flameless combustion.....	38
2.5.1	Premixed flameless combustion.....	38
2.5.2	Swirl flameless combustion .....	43
2.6	Concluding remark.....	46
<b>CHAPTER 3 METHODOLOGY.....</b>		<b>59</b>
3.1	Introduction .....	59
3.2	Experimental setup.....	60
3.2.1	Producer gas composition .....	66
3.2.2	Variables of input conditions .....	68
3.2.3	Experimental procedure .....	71
3.3	Chemical kinetic modeling strategy .....	72
3.3.1	Implementation of chemical kinetics .....	73
3.3.2	Producer gas flameless combustion modeling .....	74
3.3.3	Input variable conditions and definition .....	77
3.4	CFD simulation strategy.....	79
3.4.1	Reacting simulation strategy .....	82
3.4.2	Volume reaction modeling with global reaction mechanism.....	85
3.4.3	Significant variables of flameless combustion.....	87
3.4.3(a)	Determination of internal gas recirculation rate .....	87
3.4.3(b)	Determination of residence time .....	88

3.4.3(c)	Determination of normalized temperature uniformity...	90
3.4.3(d)	Determination of reaction regime parameters .....	91
<b>CHAPTER 4</b>	<b>EXPERIMENTAL RESULT AND DISCUSSION.....</b>	<b>93</b>
4.1	Achievement of flameless combustion .....	93
4.2	Inlet-outlet and average temperatures of combustor .....	95
4.3	Combustion characteristics under varying nozzle diameters and equivalence ratios .....	96
4.3.1	In-combustor temperature profiles.....	97
4.3.2	Flue gas temperatures and emissions .....	100
<b>CHAPTER 5</b>	<b>NUMERICAL RESULT AND DISCUSSION .....</b>	<b>105</b>
5.1	Chemical kinetic modeling.....	105
5.1.1	Formation of flameless mixture .....	106
5.1.2	Auto-ignition of PG flameless mixture.....	111
5.1.3	Determination of PG flameless combustion .....	115
5.1.4	Characteristics of PG combustion in PSR.....	119
5.2	CFD simulation .....	124
5.2.1	Model validation .....	124
5.2.2	Flow field and reaction distributions under varying equivalence ratios and nozzle diameters.....	130
5.2.2(a)	Flow field and internal gas recirculation .....	130
5.2.2(b)	Residence time distribution .....	134
5.2.2(c)	Thermal field distribution.....	137
5.2.2(d)	Reaction regime analysis.....	139
5.2.3	Combustion characteristics under varying PG properties and nozzle configurations.....	143
5.2.3(a)	Varying inlet mixture temperatures .....	146
5.2.3(b)	Varying heating value of PGs .....	152
5.2.3(c)	Varying number of nozzles.....	156

<b>CHAPTER 6</b>	<b>CONCLUSION AND RECOMMENDATION .....</b>	<b>161</b>
6.1	Experimental study on the premixed flameless combustion of PG in the cyclone combustor .....	161
6.2	Numerical analysis on the fluid dynamics and reaction regime in the cyclone combustor .....	162
6.3	Numerical determination on the realization of premixed flameless combustion .....	163
6.4	Numerical study on the premixed flameless combustion under varying PG properties and nozzle configurations.....	163
6.5	Recommendations .....	164
<b>REFERENCES.....</b>		<b>166</b>
<b>APPENDIX A: CORRECTED FLOW RATE THROUGH ORIFICE FLOWMETER</b>		
<b>APPENDIX B: CORRECTED FLOW RATE THROUGH ROTAMETER</b>		
<b>APPENDIX C: MODIFICATION OF THE AIR-FUEL NOZZLE</b>		
<b>APPENDIX D: GRID INDEPENDENT STUDY AND TURBULENT MODEL SECTION</b>		
<b>APPENDIX E: CALCULATION ROUTINE</b>		
<b>APPENDIX F: RAW EXPERIMENTAL DATA</b>		
<b>LIST OF PUBLICATIONS</b>		

## LIST OF TABLES

	<b>Page</b>
Table 2.1      The detail and obtained results of swirl-premixed burner utilizing swirl-vane and bluff-body .....	47
Table 2.2      The detail and obtained results of staged combustor investigations ..	50
Table 2.3      The detail and obtained results of flameless combustor with PG fuel .....	52
Table 2.4      The detail and obtained results of flameless combustor with other low heating value fuels, premixed mode, and swirl flow combustors .....	54
Table 3.1      Compositions of PG with lower heating value (LHV).....	68
Table 3.2      Case of investigations and input conditions.....	70
Table 3.3      Input variables of PG flameless combustion modelling .....	77
Table 3.4      Boundary conditions of simulation .....	80
Table 3.5      Model setup.....	80
Table 3.6      Kinetic rate data of each reaction.....	86
Table 3.7      Laminar flame speeds ( $S_L$ ) and flame thickness ( $\delta_F$ ) of the present PG.....	92
Table 5.1      Different reactants dilution ratio represented by letter <b>A</b> to <b>J</b> .....	116
Table 5.2      The detail of elementary reaction with reaction rate of CO formation .....	123
Table 5.3      The detail of elementary reaction with reaction rate of NO formation .....	124
Table 5.4      Operational conditions of the study .....	144
Table 5.5      Fuel properties.....	144



Table 5.6	Comparison predictions of flue gas temperature ( $T_{out}$ ) and its components between SK17 and simple reaction mechanisms with measurements .....	145
Table 5.7	Average value of reactants dilution ratio, reactive gas percentage, normalized temperature uniformity ( $T_n$ ), maximum temperature ( $T_{max}$ ), and outlet CO and NO mass fractions of varying inlet mixture temperature cases.....	147
Table 5.8	Average value of reactants dilution ratio, reactive gas percentage, normalized temperature uniformity ( $T_n$ ) and maximum temperature ( $T_{max}$ ) of varying PGs .....	153
Table 5.9	Average value of reactants dilution ratio, reactive gas percentage, normalized temperature uniformity ( $T_n$ ) and maximum temperature ( $T_{max}$ ) for varying number of nozzles .....	157

## LIST OF FIGURES

	Page
Figure 1.1 Power generation share for Southeast Asia region for 2000 and 2013 (IEA, 2015) .....	2
Figure 1.2 Typical outline of producer gas utilization as alternative fuel.....	3
Figure 1.3 Comparison of the features of traditional combustion (a) and flameless combustion (b) (Milani, 2001).....	6
Figure 2.1 Comparison between combustion processes with (solid line) and without (dashed line) heat recirculation (Belmont, 2014) .....	13
Figure 2.2 Different combustion regimes based on O <sub>2</sub> concentration, recirculation ratio, and reactant temperature (Rao and Levy, 2010) .....	15
Figure 2.3 Combustion regimes based on Borghi diagram $Da$ against $Re_t$ (Khalil and Gupta, 2017): $L_0$ = integral length scale, $\delta_L$ = flame thickness, and $L_k$ = Kolmogorov length scale.....	16
Figure 2.4 (a) Adiabatic flame temperature and (b) laminar flame speed at stoichiometric mixture of H <sub>2</sub> /CO/CH <sub>4</sub> /air as a function of CO and H <sub>2</sub> additions (Cheng et al., 2011) .....	19
Figure 2.5 Combustion stability diagram for producer gas (Hernandez et al., 2012).....	21
Figure 2.6 (a) Schematic arrangement of burner components (Panwar et al., 2011), (b) swirl vane and (c) bluff body (Bhoi and Channiwala, 2008) .....	22
Figure 2.7 (a) Schematic drawing of four air-staged burner (Sukumaran and Kong, 2013) and (b) continuous air staging (COSTAIR) (Al-Halbouni et al., 2007) for producer gas combustion .....	26

Figure 2.8	(a) Schematic drawing of non-premixed cyclone combustor (Dattarajan et al., 2014) and (b) premixed cyclone combustor (Al-Attab and Zainal, 2011).....	28
Figure 2.9	Schematic drawing of ZVC chamber (Szewczyk et al., 2015) .....	30
Figure 2.10	Schematic drawing of conical combustor (Kumar et al., 2005).....	31
Figure 2.11	FLOX combustor model and its schematic drawing (Zornek et al., 2015).....	32
Figure 2.12	(a) Co-flow jets configuration, (b) cross-flow-jets combustion configuration, and (c) cyclonic cross-jets configuration with flameless pictures at upper combustion chambers (Kwiatkowski and Mastorakos, 2016).....	34
Figure 2.13	Submerged flame from alumina balls packed bed burner (Chung Ho, 2012) .....	35
Figure 2.14	Comparison of (a) non-premixed flameless combustion and (b) premixed flameless combustion system.....	39
Figure 2.15	Schematic drawing of premixed flameless combustor (Mi et al., 2009) .....	41
Figure 2.16	Schematic drawing of swirl combustor for colorless distributed combustion (Khalil and Gupta, 2014a) .....	44
Figure 2.17	Cyclonic combustor and its schematic diagram (Sorrentino et al., 2017) .....	45
Figure 3.1	Flowchart of methodology used in this study .....	59
Figure 3.2	Schematic diagram of the experimental setup .....	62
Figure 3.3	Fixed-bed downdraft gasifier .....	63
Figure 3.4	Schematic drawing of high temperature cyclone separator .....	64
Figure 3.5	Orifice meter and its schematic diagram.....	64
Figure 3.6	Thermocouples data logger.....	65
Figure 3.7	Kane exhaust gas analyser .....	65

Figure 3.8	(a) Premixed cyclone combustor model, (b) schematic dimensions in mm, and (c) inlet nozzle.....	66
Figure 3.9	(1) Gas Chromatograph Agilent Model 4890D with (2) helium tank and (3) compressed air tank .....	67
Figure 3.10	Schematic diagram of the CHEMKIN library structure (Kee et al., 1996) .....	73
Figure 3.11	Schematic model of PG flameless combustion process in Chemkin package.....	75
Figure 3.12	The modelled grid for computational domain.....	79
Figure 4.1	Flame photographs of preheating step with LPG combustion and transition from flame into flameless combustion mode for a case of nozzle diameter of 50 mm .....	94
Figure 4.2	Temperature positions along combustion chamber height (Z) .....	95
Figure 4.3	Profiles of inlet temperature of fuel/air mixture ( $T_{in}$ ), average temperature ( $T_{ave}$ ), exhaust gas temperature ( $T_{out}$ ) against combustion air flow rate.....	96
Figure 4.4	Temperature profile along axial combustor height for different nozzle diameters at equivalence ratio of 1.11 .....	97
Figure 4.5	Temperature profile along axial combustor height for different nozzle diameters at equivalence ratio of 0.89 .....	98
Figure 4.6	Temperature profile along axial combustor height for different nozzle diameters at equivalence ratio of 0.74 .....	98
Figure 4.7	Temperature profile along axial combustor height for different nozzle diameters at equivalence ratio of 0.63 .....	99
Figure 4.8	Flue gas temperature at different equivalence ratios for nozzle diameter of 50 mm, 40 mm, and 30 mm .....	100
Figure 4.9	CO emissions at different equivalence ratios for nozzle diameter of 50 mm, 40 mm, and 30 mm .....	101
Figure 4.10	NO <sub>x</sub> emissions at different equivalence ratios for nozzle diameter of 50 mm, 40 mm, and 30 mm .....	102

Figure 5.1	Chemical kinetic modelling for laminar flame speed ( $S_L$ ) of PG.....	105
Figure 5.2	Chemical kinetic modelling for adiabatic temperature ( $T_{ad}$ ) of PG .	106
Figure 5.3	Auto-ignition temperature against reactants dilution ratio for different fresh reactants equivalence ratios.....	107
Figure 5.4	Flameless mixture temperature against reactants dilution ratio for different fresh reactants temperatures at equivalence ratio of 0.6 ...	108
Figure 5.5	Flameless mixture temperature against reactants dilution ratio for different fresh reactants temperatures at equivalence ratio of 1.0 ...	108
Figure 5.6	Flameless mixture temperature against reactants dilution ratio for different fresh reactants temperatures at equivalence ratio of 1.2 ...	109
Figure 5.7	Oxygen mole fraction as a function of reactants dilution ratio for different fresh reactants temperatures at equivalence ratio of 0.6 ...	110
Figure 5.8	Oxygen mole fraction as a function of reactants dilution ratio for different fresh reactants temperatures at equivalence ratio of 1.0 ...	110
Figure 5.9	Oxygen mole fraction as a function of reactants dilution ratio for different fresh reactants temperatures at equivalence ratio of 1.2 ...	111
Figure 5.10	Ignition delay time as a function of reactants dilution level of flameless mixture for different $T_{FR}$ at $\phi = 1.0$ .....	112
Figure 5.11	Ignition delay time as a function of reactants dilution level of flameless mixture for different $\phi$ at $T_{FR}$ of 300 K .....	113
Figure 5.12	Evolution of temperature and mole fraction of radical species $HO_2$ , $OH$ and $H$ for without dilution case ( $R_{dil} = 0.0$ ) at $T_{FR}$ of 300 K and $\phi$ of 1.0 .....	114
Figure 5.13	Evolution of temperature and mole fraction of radical species $HO_2$ , $OH$ and $H$ for dilution case ( $R_{dil} = 0.9$ ) at $T_{FR}$ of 300 K and $\phi$ of 1.0 .....	114
Figure 5.14	Combustion regions of PG in PSR for different fresh reactants temperatures at equivalence ratio of 0.6 .....	117

Figure 5.15	Combustion regions of PG in PSR for different fresh reactants temperatures at equivalence ratio of 1.0 .....	118
Figure 5.16	Combustion regions of PG in PSR for different fresh reactants temperatures at equivalence ratio of 1.2 .....	118
Figure 5.17	Temperature in PSR against $T_{FR}$ ; comparison between traditional, $R_{dil} = 0$ , and flameless, $R_{dil} = 0.9$ , combustion modes at $\phi = 0.6$ .....	119
Figure 5.18	Temperature in PSR against $T_{FR}$ ; comparison between traditional, $R_{dil} = 0$ , and flameless, $R_{dil} = 0.9$ , combustion modes at $\phi = 1.0$ .....	120
Figure 5.19	Temperature in PSR against $T_{FR}$ ; comparison between traditional, $R_{dil} = 0$ , and flameless, $R_{dil} = 0.9$ , combustion modes at $\phi = 1.2$ .....	120
Figure 5.20	CO mole fraction against $T_{FR}$ ; comparison between traditional combustion, $R_{dil} = 0$ , and flameless, $R_{dil} = 0.9$ , combustion modes at $\phi = 1.0$ .....	121
Figure 5.21	NO mole fraction against $T_{FR}$ ; comparison between traditional combustion, $R_{dil} = 0$ , and flameless, $R_{dil} = 0.9$ , combustion modes at $\phi = 1.0$ .....	122
Figure 5.22	(a) temperature, (b) CO, and (c) CO <sub>2</sub> profiles along the central combustor height for three grid structures for the case of $\phi = 0.89$ and $d = 50$ mm .....	126
Figure 5.23	Schematic of different planes and a line along the combustor for CFD result extractions .....	127
Figure 5.24	Comparison between temperature profiles of RNG $k-\varepsilon$ and RSM models with experiment for the case of $\phi = 0.89$ and $d = 50$ mm....	127
Figure 5.25	Comparison between temperature profiles of FR/ED, ED, and EDC models with experiment for the case of $\phi = 0.89$ and $d = 50$ mm .....	128
Figure 5.26	Comparison between temperature profiles of CFD predictions and experiments: (a) $\phi = 1.11$ , (b) $\phi = 0.89$ , (c) $\phi = 0.74$ , (d) $\phi = 0.63$ , and (e) for output temperature ( $T_{out}$ ) against $\phi$ .....	129

Figure 5.27	Axial velocity contours and vectors field coloured by axial velocity for case of equivalence ratio of 0.89 with nozzle diameter of 30 mm .....	130
Figure 5.28	Reactants dilution ratio for keeping nozzle diameter of 30 mm and varying $\phi$ .....	132
Figure 5.29	Reactants dilution ratio for keeping $\phi = 0.89$ and varying nozzle diameter.....	132
Figure 5.30	Average turbulent intensity for keeping nozzle diameter of 30 mm and varying $\phi$ .....	133
Figure 5.31	Average turbulent intensity for keeping $\phi = 0.89$ and varying nozzle diameter .....	134
Figure 5.32	Variation of RTD curves for different equivalence ratios .....	135
Figure 5.33	Variation of RTD curves for different nozzle diameters .....	135
Figure 5.34	Mean residence times for keeping nozzle diameter of 30 mm and varying $\phi$ .....	136
Figure 5.35	Mean residence times for keeping $\phi = 0.89$ and varying nozzle diameter.....	136
Figure 5.36	Uniformity temperature contour for the case of nozzle diameter of 30 mm and equivalence ratio of 0.89.....	137
Figure 5.37	Normalized temperature uniformity ( $T_n$ ) for keeping nozzle diameter of 30 mm and varying $\phi$ .....	138
Figure 5.38	Normalized temperature uniformity ( $T_n$ ) for keeping $\phi = 0.89$ and varying nozzle diameter .....	138
Figure 5.39	Variation of $\delta_F$ , $\tau_{chem}$ and $\tau_{flow}$ for different equivalence ratios .....	139
Figure 5.40	Variation of $\delta_F$ , $\tau_{chem}$ and $\tau_{flow}$ for different nozzle diameters .....	139
Figure 5.41	Damköhler ( $Da$ ) distribution contours for the case of nozzle diameter of 30 mm and equivalence ratio of 0.89.....	140
Figure 5.42	Karlovitz ( $Ka$ ) distribution contours for the case of nozzle diameter of 30 mm and equivalence ratio of 0.89.....	141

Figure 5.43	Predicted reaction regime of premixed producer gas flameless combustion under varying equivalence ratios with nozzle diameter of 30 mm .....	142
Figure 5.44	Predicted reaction regime of premixed producer gas flameless combustion under varying nozzle diameters with equivalence ratio of 0.89 .....	143
Figure 5.45	Axial velocity profiles along central combustion chamber for varying inlet mixture temperatures ( $T_{in}$ ) .....	146
Figure 5.46	Temperature contours for different inlet mixture temperature ( $T_{in}$ )	149
Figure 5.47	Axial temperature profiles along central combustion chamber for varying inlet mixture temperatures ( $T_{in}$ ) .....	150
Figure 5.48	Axial CO mass fraction profiles along central combustion chamber for varying inlet mixture temperatures ( $T_{in}$ ).....	151
Figure 5.49	Axial NO mass fraction profiles along central combustion chamber for varying inlet mixture temperatures ( $T_{in}$ ).....	152
Figure 5.50	Various temperature contours for different PG fuels.....	154
Figure 5.51	Maximum CO and NO mass fractions at combustor exit against varying heating value of PGs .....	155
Figure 5.52	Configuration of nozzles for each case .....	156
Figure 5.53	Temperature distribution contours of each nozzle configuration ....	158
Figure 5.54	Variation of axial temperature profiles of each nozzle configuration .....	159
Figure 5.55	CO and NO mass fractions at combustion chamber exit against number of nozzles .....	160



## LIST OF SYMBOLS

$A$	Pre-exponential factor of Arrhenius equation
$A_{in}$	Cross-section area of inlet combustor
$a, b, c, \dots z$	Number of moles
$C(t)$	Tracer concentration
$C_{\xi}$	Constant of Eddy Dissipation Concept Model
$C_{\tau}$	Constant of Eddy Dissipation Concept Model
$d$	Nozzle diameter
$Da$	Damköhler number
$D_C$	Combustor diameter
$d_{ex}$	Exit combustor diameter
$E_a$	Activation energy
$E(t)$	Exit age distribution of tracer concentration
$F/A$	Actual fuel to air ratio
$(F/A)_{st}$	Stoichiometric fuel to air ratio
HHV	Higher heating value
$J_i$	Diffusion flux of species $i$
$J_{in}$	Initial jet momentum rate
$K$	Reaction rate constant of Arrhenius equation
$k$	Turbulent kinetic energy
$Ka$	Karlovitz number
$K_V$	Recirculation factor
$l_0$	Integral length scale
LHV	Lower heating value
$M_A$ or $m_A$	Mass flow rate of combustion air

$m_{A/F}$	Mass flow rate of premixed air/fuel
$M_E$ or $m_{eg}$	Mass flow rate of exhaust gas recirculation
$M_F$ or $m_F$	Mass flow rate of fuel
$m_{in}$	Inlet mass flow
$m_{up}$	Upwards mass flow gas
$N$	Number of nozzles
$Q_A$	Sensible heat of combustion air
$Q_F$	Chemical enthalpy of fuel
$Q_{eg}$	Sensible heat of flue gas
$Q_{wall}$	Wall heat losses
$R_C$	Outer radius of combustor
$R$	Universal gas constant
$r$	Radial location of combustor
$R_{dil}$	Reactants dilution ratio
$Re_t$	Turbulence Reynolds number
$R_i$	Mean source term of species $i$
$S_g$	Geometrical swirl number
$S_n$	Swirl number
$S_L$	Laminar flame speed
$S_{L,ref}$	Reference laminar flame speed
$T_0$	Temperature at beginning condition
$\Delta T$	Temperature increment during combustion process
$\Delta T(t)$	Temperature increment as function of time
$T_{ad}$	Adiabatic flame temperature
$T_{ave}$	Average combustor temperature
$T_C$	Combustion temperature
$T_{FR}$	Fresh reactants temperature

$T_i$	Temperature at location $i= 1, 2, 3 \dots$
$T_{ig}$	Auto-ignition temperature
$T_{in}$	Inlet reactants temperature
$T_{mix}$	Flameless mixture
$T_n$	Normalized temperature uniformity
$T_{out}$	Combustor outlet temperature (flue gas temperature)
$T_{PG}$	Producer gas temperature
$T_{ref}$	Reference temperature condition
$T_u$	Temperature uniformity
$u$	Axial velocity
$\vec{v}$	Vector velocity
$V$	Combustor (reactor) volume
$V_{in}$	Inlet reactants velocity
$V_{rms}$	Root-mean-square fluctuating velocity
$v_z$	Velocity along Z-direction
$w$	Tangential velocity
$X_i$	Concentration of species $i$
$Y_i$	Mass fraction of species $i$
$\tau_{flow}$	Characteristic flow time
$\tau_{chem}$	Characteristic chemical time
$\tau_k$	Characteristic Kolmogorov time
$\tau$	Residence time
$\tau_m$	Mean residence time
$\phi$	Equivalence ratio
$\varepsilon$	Turbulent dissipation rate
$\alpha$	Thermal diffusivity

$\nu$	Turbulent kinematic viscosity
$\rho$	Density of gas mixture
$\rho_{in}$	Inlet gas mixture density
$\delta_F$	Flame thickness
$\beta$	Temperature exponent rate of Arrhenius equation
$\zeta$	Fine structure scale of Eddy Dissipation Concept model
$\gamma$	Correlation factor of power law equation
$\eta_{th}$	Thermal efficiency of combustor

## LIST OF ABBREVIATIONS

A	Air
CDC	Colorless Distributed Combustion
CFD	Computational Fluid Dynamics
CHBR	Closed Homogeneous Batch Reactor
CHP	Combined Heat and Power Generation System
COSTAIR	Continuous Air Staging Combustor
CRN	Chemical Reactors Network
E	External Heat/Exhaust Gas Recirculation
EDM	Eddy Dissipation Model
EDC	Eddy Dissipation Concept Model
F	Fuel
FC	Flameless Combustion
FLOX	Flameless Oxidation
FR/ED	Finite Rate/Eddy Dissipation Model
GUI	Graphical User Interface
HiTAC	High Temperature Air Combustion
HTC	High Temperature Combustion
I	Internal Heat/Exhaust Gas Recirculation
IEA	International Energy Agency
LPG	Liquefied Petroleum Gas
MILD	Moderate or Intense Low-oxygen Dilution
PG	Producer Gas
RNG	Renormalization Group Turbulent Model
RSM	Reynolds Stress Turbulent Model

PSR	Perfectly Stirred Reactor
RTD	Residence Time Distribution
TC	Traditional Combustion
TI	Turbulence Intensity
UC	Unstable Combustion
WSGGM	Weighted-Sum-of-Gray-Gases Model
ZVC	Zonal Volumetric Combustion Chamber

# **PEMBAKARAN TANPA NYALAAAN API PRACAMPUR BAGI GAS PENGELUAR DALAM SEBUAH PEMBAKAR SIKLON**

## **ABSTRAK**

Mod pembakaran konvensional gas pengeluar (PG) menghadapi masalah nyalaan yang tidak stabil, kadar pembakaran yang rendah, dan kemerosotan output kuasa disebabkan kandungan pemanasannya yang rendah. Pembakaran tanpa nyalaan ialah teknik pembakaran yang membawa harapan untuk meningkatkan prestasi proses pembakaran. Walau bagaimanapun, teknik ini masih kurang lazim digunakan dengan PG. Kajian ini bertujuan menyelidik pembakaran tanpa nyalaan pracampuran PG. PG yang diterbitkan daripada pengelasan bongkah kayu getah dibakar di dalam pembakar siklon pracampuran. Kemudian, simulasi berangka dilakukan untuk memahami proses-proses kinetik kimia dan ciri-ciri pembakarannya. Hasil uji kaji menunjukkan bahawa proses pembakaran optimum dicapai apabila muncung salur masuk berdiamater 30 mm digunakan dengan nisbah kesetaraan 0.89 berserta suhu gas serombong 1096.33 K dan CO minimum sebanyak 133.3 ppm sementara NO<sub>x</sub> bernilai 402.3 ppm. Analisis kinetik kimia dan simulasi ciri-ciri dinamik bendalir (CFD) telah digunakan untuk menentukan pencapaian pembakaran tanpa nyalaan berdasarkan nisbah pencairan bahan tindak,  $R_{dil} > 0.6$ , keseragaman suhu ternormal,  $T_n < 15\%$ , dan aturan tindak balasnya. Hasil CFD juga mendedahkan bahawa kenaikan suhu bahan tindak daripada 400 K kepada 700 K berjaya menyeragamkan lagi agihan suhu tetapi juga meningkat CO daripada 170 ppm kepada 401.19 ppm dan NO daripada 12.7 ppm kepada 58.9 ppm. Kenaikan nilai pemanasan bahan api telah mengurangkan keseragaman agihan suhu dengan ketara. CO berkurang daripada 170.01 ppm kepada 21.88 ppm manakala NO bertambah daripada 13 ppm kepada 795 ppm apabila nilai

pemanasan dinaikkan daripada 4 MJ/m<sup>3</sup> kepada 11.6 MJ/m<sup>3</sup>. Apabila angka muncung dinaikkan daripada 1*N* kepada 4*N*, keseragaman agihan suhu berkurang sedikit. CO berkurang daripada 170.01 ppm kepada 103.249 ppm manakala NO bertambah daripada 12.7 ppm kepada 47.34 ppm.



# **PREMIXED FLAMELESS COMBUSTION OF PRODUCER GAS IN A CYCLONE COMBUSTOR**

## **ABSTRACT**

Conventional combustion mode of producer gas (PG) encounters flame instability, low burning rate, and dropping in power output due to its low heating content. Flameless combustion is a promising combustion technique for improving performance of the combustion process. However, its application with PG remains much less common. This study aims to investigate premixed flameless combustion of PG. PG derived from a gasification of rubber wood blocks was combusted in a premixed cyclone combustor. Then, numerical simulation was conducted to gain insight into the chemical kinetics processes and its combustion characteristics. Experimental results showed that the optimum combustion process was achieved for the case of inlet nozzle diameter of 30 mm and equivalence ratio of 0.89 with flue gas temperature of 1096.33 K and minimum CO of 133.3 ppm while NO<sub>x</sub> emission was 402.3 ppm at this operating point. Chemical kinetics analysis and computational fluid dynamics (CFD) simulation were implemented to determine the achievement of flameless combustion based on reactants dilution ratio,  $R_{dil} > 0.6$ , normalized temperature uniformity,  $T_n < 15\%$ , and its reaction regime. The CFD results also revealed that increasing inlet reactants temperature from 400 K to 700 K was beneficial for more uniformity of temperature distribution, but it resulted in increasing CO from 170 ppm to 401.19 ppm and NO from 12.7 ppm to 58.9 ppm. Increasing the heating value of fuel significantly decreased the temperature distribution uniformity. CO decreased from 170.01 ppm to 21.88 ppm while NO increased from 13 ppm to 795 ppm when increasing heating value from 4 MJ/m<sup>3</sup> to 11.6 MJ/m<sup>3</sup>. For increasing

number of the nozzle from 1*N* to 4*N*, it slightly decreased the temperature distribution uniformity. CO decreased from 170.01 ppm to 103.249 ppm while NO increased from 12.7 ppm to 47.34 ppm.

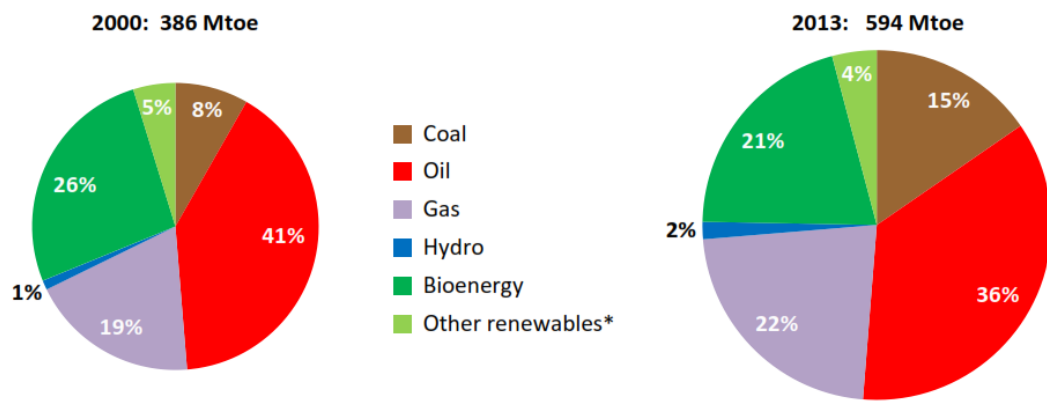
# CHAPTER 1

## INTRODUCTION

### 1.1 Overview

The world's energy consumption is increasing steadily with continuous population and economic growth. Specifically, in Southeast Asia, the demand for energy has been increased by more than 50% from 2000 to 2013 and it will be increased up to 80% in 2040 (IEA, 2015). It is noticeably observed that the biggest share of power generations is derived mainly from utilizing fossil fuels such as coal, gas, and oil, as shown in Figure 1.1.

In the power generation point of view, combustion constitutes a primary requisite for fuel to energy conversion. However, the combustion results in environmental problems, especially greenhouse gas emissions (Hosseini and Wahid, 2014). To mitigate these concerns, alternative fuels derived from renewable energy source are sorted as one of the potential options (Herbert and Krishnan, 2016; Hosseini et al., 2013; Muench, 2015). Combustion of alternative fuels with low carbon containing (and thus its low heating value) will results in low greenhouse gas emissions in comparison with the fossil fuel. Biomass has been considered as one of the biggest renewable energy sources which can be utilized mainly for producing alternative fuels to mitigate the dependency of the fossil fuel (Demirbas, 2005; Herbert and Krishnan, 2016; Muench, 2015; Panwar et al., 2012; Ruiz et al., 2013). Furthermore, utilization of biomass energy has an advantage in terms of low carbon footprint energy for reducing the negative effects of the environmental issues, especially net CO<sub>2</sub> emissions which could be suppressed throughout the bio-cycle (Yeoh et al., 2018).



\* includes solar PV, wind, and geothermal; Note: Mtoe = million tonnes of oil equivalent by 1 toe = 41.87 GJ (Giga Joules)

Figure 1.1 Power generation share for Southeast Asia region for 2000 and 2013 (IEA, 2015)

## 1.2 Producer gas as an alternative gas fuel

Outline of typical processes of the conversion of biomass to energy from gasification to downstream utilizations is illustrated in Figure 1.2. Basically, biomass can be directly fired to generate heat and power. However, it can be converted into more useful energy form in terms of gaseous fuel known as producer gas (PG) or synthesis gas, which can be used for firing and operating the engines. PG derives from partial combustion of any biomass through a gasification process where a mixture of both combustible and non-combustible gases is formed (Belgiorno et al., 2003; Dudyński et al., 2012; Sansaniwal et al., 2017; Widjaya et al., 2018).

By an air-blown gasification process under operating temperature below 1200°C, the gas composition will include carbon monoxide (CO), hydrogen (H<sub>2</sub>), methane (CH<sub>4</sub>), and incombustible species (N<sub>2</sub>, H<sub>2</sub>O, and CO<sub>2</sub>) as well as small oxygen concentrations (O<sub>2</sub>) (Al-Attab et al., 2015; Al-Attab and Zainal, 2011, 2017; Zainal, et al., 2002; Zainal et al., 2010). The concentration of these species depends upon the type of gasification process, gasifier, biomass material, and gasifying agent (Couto et

al., 2013; Lapuerta et al., 2008; Rafidah et al., 2011; Weerachanchai et al., 2009; Zainal et al., 2010). As demonstrated by Huynh and Kong (2013), using oxygen-enriched air/steam gasification can significantly enhance  $H_2/CO$  ratio of PG mixture. The increase of  $H_2/CO$  ratio is beneficial for enhancement of PG quality by increasing its heating value (Basu, 2010).

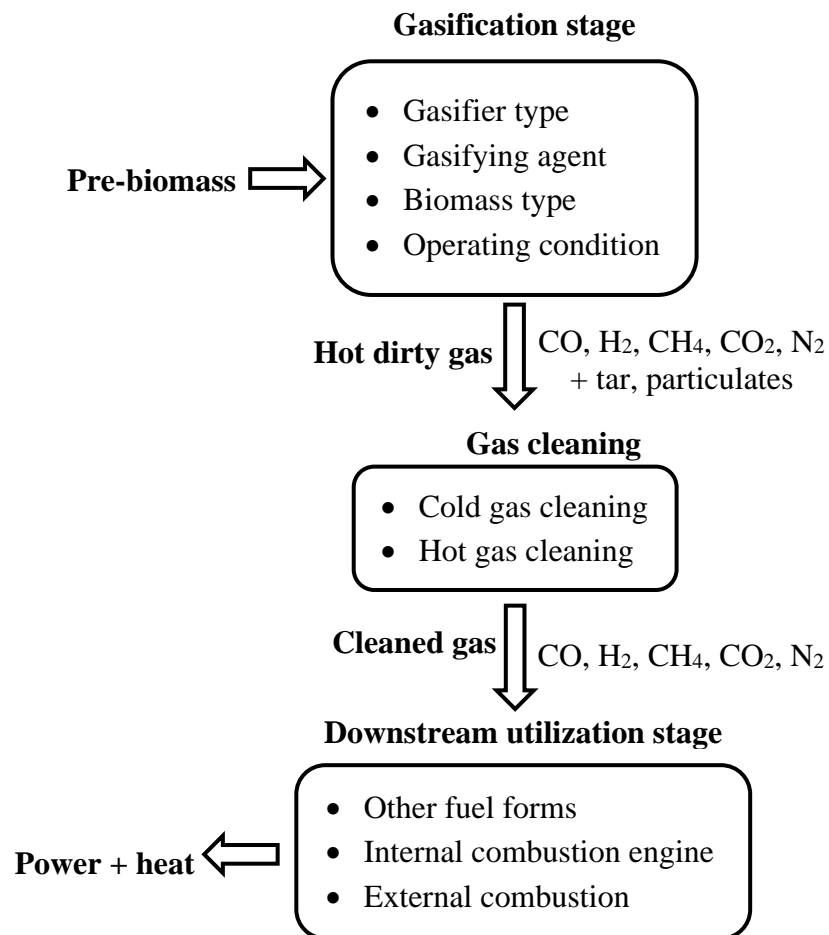


Figure 1.2 Typical outline of producer gas utilization as alternative fuel

From Figure 1.2, the final stage of the downstream utilization, combustion process plays a key role in the PG to power and energy conversion. From an economic point of view for small-scale application of the combined heat and power generation (CHP) system, firing in a combustion chamber and utilizing it in combination with external combustion engines is a remarkable option (De Mena et al., 2017; Rentizelas et al., 2009; Rokni, 2014). By this approach, raw PG has no need to be deeply cleaned (De Mena et al., 2017) due to the firing in a combustion chamber is not very sensitive to contaminates the raw PG as in internal combustion engine applications and thus, specific gas cleaning/cooling systems can be eliminated. However, with different combustible gas compositions and uncertain heating value of PG, the optimized combustion chamber as well as flexible and efficient combustion techniques need to be addressed while utilizing PG via a combustion process (Ghenai, 2010; Kwiatkowski et al., 2012; 2013; Oliveira et al., 2012).

### **1.3 Flameless combustion as a promising combustion for PG fuel**

#### **1.3.1 Definition of flameless combustion**

Combustion with invisible flame called “Flameless Combustion” is a modern combustion technology, which can fulfil the requirement of high thermal efficiency and low pollutant emissions (Xing et al., 2017). Flameless combustion can also be found in different names such as “High Temperature Air Combustion (HiTAC)” (Tsuji et al., 2003), “Flameless Oxidation (FLOX) combustion” (Wünning and Wünning, 1997), “Moderate or Intense Low-oxygen Dilution (MILD) combustion” (Cavaliere and De Joannon, 2004), and “Colorless Distributed Combustion (CDC)” (Arghode and Gupta, 2010). However, these combustion methods rely on the same principle that the

combustion process is operated under low oxygen reactive environment by means of high preheating and diluting fresh reactants before its reaction and the combustion process is carried out by entirely distributed auto-ignition of fuel/air mixture. Therefore, the achievement of flameless combustion is based on high preheating with dilution of fresh reactants where: (1) the temperature of the fresh reactants must be higher than auto-ignition temperature of the fuel (Cavaliere and de Joannon, 2004; Wüning and Wüning, 1997) and (2) the local reactants mixture must be diluted by inert species into less than 15% oxygen concentration (Khalil and Gupta, 2014; Lezcano et al., 2012; Mancini et al., 2007).

During flameless combustion process, combustion volume is occupied by distributed reaction and uniform temperature field, leading to invisible flame with disappearing flame front and merging the main reaction zone into the post-flame zone. Although flameless combustion mode operates under high temperature environment (higher than the auto-ignition point of the fuel), its peak combustion temperature is suppressed, which is much lower than that of the traditional combustion mode. This is because of the combustion volume is entirely diluted by hot combustion products, leading to slower reaction rates and then, lower combustion temperature. Figure 1.3 illustrates the different features of flameless combustion to traditional combustion mode (Milani, 2001).

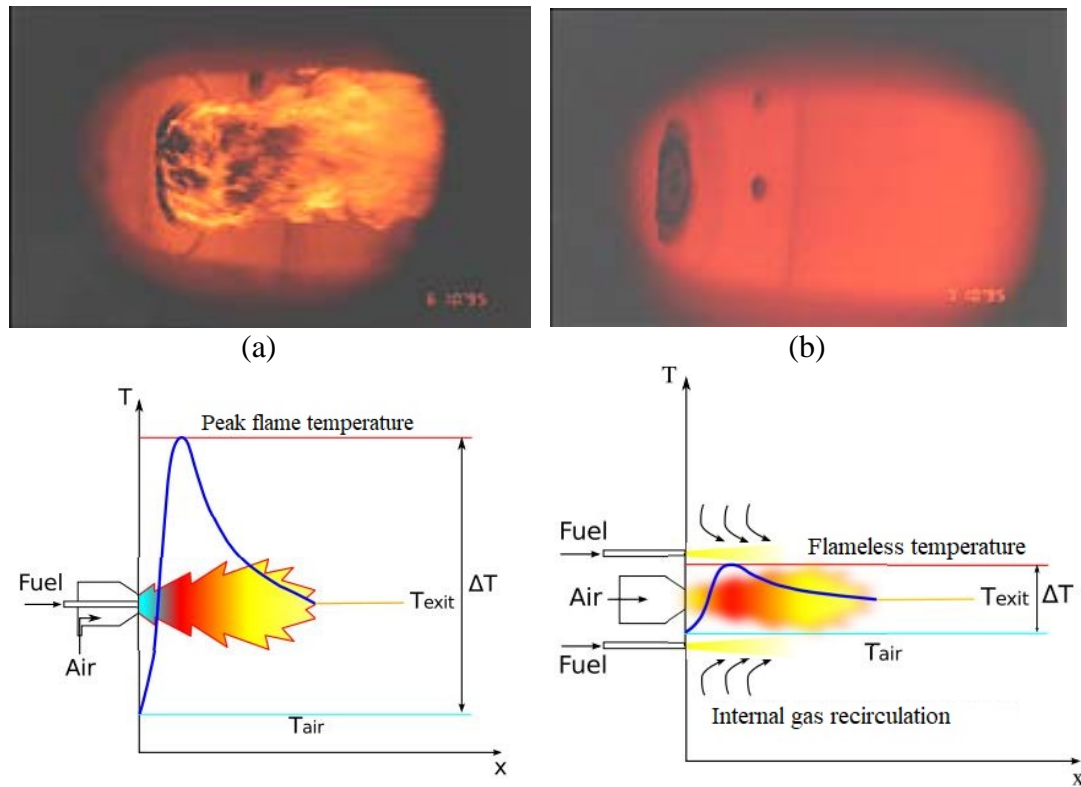


Figure 1.3 Comparison of the features of traditional combustion (a) and flameless combustion (b) (Milani, 2001)

### 1.3.2 Benefits and application status of flameless combustion

High degree of preheating combined with large thermal distributions (high temperature of both reactant and furnace) allow for fully oxidized fuel/air mixture, leading to complete combustion (low CO emission). Also, thermal efficiency and flame stabilization are improved considerably in comparison with traditional combustion mode (Gupta, 2004). Furthermore, lower peak combustion temperature results in lower NO<sub>x</sub> emissions due to suppression of NO thermal formations (Abuelnuor et al., 2014).



Flameless combustion is first applied for industrial furnace to reduce NO<sub>x</sub> emission and enhance performance of the combustion system where regenerative heat exchangers are used to absorb waste heat of combustion products and transfer it back to the combustion zone. This recovering heat can be directly translated into a term of fuel saving, which demonstrated by experiments (Katsuki and Hasegawa, 1998; Tsuji et al., 2003) that the fuel saving can be increased up to 30%, corresponding to the same amount of CO<sub>2</sub> reduction on the basis of correlation between fuel consumption, CO<sub>2</sub> production, and fuel saving. NO<sub>x</sub> emission from flameless combustion mode can be decreased by up to 80% in comparison with traditional mode (Abuelnuor et al., 2014). Meantime, application of flameless combustion in an industrial boiler can be found in investigation of Kawai et al. (2002). Currently, flameless combustion has been focussed to gas turbine combustors (Khidr et al., 2017; Perpignan et al., 2018; Xing et al., 2017).

Flameless combustion presents a successful combustion technology to improve flame stability with high thermal field uniformity. This can be considered as a promising combustion method for low heating value fuel. Flame instability and low burnt-out rate combustions due to low heating value of the fuel can be mitigated by the high thermal field uniformity of flameless combustion technique. In particular, for PG fuel, high levels of preheating and dilution are already present in the PG through the gasification process. This will comply with the principle of flameless combustion. The raw PG generated in an air-blown gasifier has an exit temperature higher than 700°C (Kwiatkowski et al., 2013) and consists of N<sub>2</sub> and CO<sub>2</sub> as inert gases of over 50% in its mixture (Al-Attab and Zainal, 2014), making PG a suitable fuel for fuelling flameless combustion.

#### **1.4 Problem statement**

Utilizing PG via combustion process suffers difficulties such as (1) with low heating value of PG, the combustion process encounters flame instability and low burnout rate, (2) low heating value of PG can leads to low power output and drop in overall combustion efficiency, and (3) the combustion process of PG also suffers high dilution of inert species ( $N_2$  and  $CO_2$ ) and various combustible species ( $CO$ ,  $H_2$ , and  $CH_4$ ), leading to difficulties for optimization of burner configurations as well as determination of the combustion conditions.

In this sense, combustion of PG in an ordinary combustion system cannot guarantee sufficiently flame stability and low pollutant emissions. Although flameless combustion technology has the great performance to fulfil these requirements, its application extending to PG fuel remains much less common. Especially, premixed flameless combustion of PG in a swirl flow combustor has not yet been investigated. There is a wide variety of the firing systems utilized premixed combustion mode from small-scale power generation plant to industrial furnace applications (Peters, 2004; Turns, 2000). Premixed combustion strategy allows for good mixing result with a certain ratio of fuel/air mixture, which is better to control operating combustion conditions and to achieve low polluting emissions. If those systems can operate in flameless combustion mode with PG fuel, performance of the combustion system could be considerably improved with an outstanding reduction of polluting emissions. Hence, further investigation on this regard is needed.

## **1.5 Objective of study**

The focus of this study is to fulfil the gap of premixed flameless combustion application with PG fuel. Combination of a gasifier with a cyclone combustor to operate premixed swirl flameless combustion of PG is performed in this study. Both the experimental and numerical investigations are employed, as the following objectives:

- 1) To investigate experimentally the premixed combustion characteristics operated under flameless combustion mode with producer gas fuel in a cyclone combustor.
- 2) To conduct numerical simulation on the fluid dynamics, internal dilution ratio, and reaction regime in the combustor.
- 3) To determine numerically the initial conditions of fresh premixed reactants that influence the realization of producer gas flameless combustion, its auto-ignition process, and the combustion process in a chemical reactor.
- 4) To investigate numerically the effects of producer gas properties and nozzle configurations on the combustion characteristics of producer gas flameless mode.

## 1.6 Scope and limitation

The scope of the present research work can be summarized as follows:

- 1) In the experiment, producer gas is produced using an air-blown fixed-bed down draft gasifier with its thermal capacity within 50 – 222 kW<sub>th</sub> with respect to producer gas productions, using rubber wood blocks with maximum block length of about 15 cm as solid fuel for the gasifier.
- 2) Hot producer gas after the gasifier is cleaned by using an insulated cyclone separator in order to remove ash and particles from the raw producer gas mixture before it is being used as fuel for the combustion process.
- 3) The gasification and combustion processes are operated under atmospheric condition where both gasifying air and combustion air are supplied to the system at ambient temperature and pressure.
- 4) The producer gas fuel is burned in a premixed cyclone combustor and the combustion process characterizes based on temperature profile along the combustion chamber, flue gas temperature, and pollutant emissions, operating at the thermal power input of the fuel of about 90 kW<sub>th</sub> under the condition of temperature of 300 K and pressure of 101325 Pa.
- 5) Temperature is measured using K-type thermocouples and exhaust gas analyser type is used to record the pollutant emissions such as CO (%), CO<sub>2</sub> (%), O<sub>2</sub> (%), and NO<sub>x</sub> (ppm), however, this exhaust gas analyser cannot measure Sulphur oxide (SO<sub>x</sub>) and unburn hydrocarbon (UHC).
- 6) Numerical simulation for investigating flameless combustion and auto-ignition process of producer gas fuel is conducted by using ANSYS

Chemkin-Pro 17.0 in combination with the detail reaction mechanism of GRI-Mech., 3.0. CFD simulation for characterizing the flameless combustion of producer gas in a premixed cyclone combustor is performed using Fluent CFD code of ANSYS software 17.2.

- 7) Since CFD simulation with the detail reaction mechanism consumes expensively computational task, global reaction mechanisms based on the default values in the ANSYS Fluent software and semi-detail reaction mechanism of skeletal 17 species are considered for the CFD simulation.

## **1.7 Thesis outline**

Numerical and experimental studies are both carried out and presented in this thesis. Chapter 2 provides literature reviews involved with the development of PG combustion technologies, including the investigations of flameless combustion, which operated in swirl flow and premixed combustors. Chapter 3 describes methodology used in this study. Experiments on flameless combustion of PG fuel in a premixed cyclone combustor and its results are described in Chapter 4. The essential conditions for the realization of PG flameless combustion are estimated through chemical kinetics modelling. Furthermore, the auto-ignition and combustion processes of PG under dilution (flameless combustion mode) and non-dilution (traditional combustion mode) cases are described in Chapter 5. CFD simulations to gain results of flow field inside a cyclone combustor and flameless combustion characteristics as well as the effects of PG properties and nozzle configurations on the premixed flameless combustion characteristics of PG are also presented in Chapter 5. Conclusions of the study are summarized in Chapter 6.

## **CHAPTER 2**

### **LITERATURE REVIEW**

#### **2.1 Improvement of combustion performance**

The concept of flue gas recirculation to preheat reactants, especially in preheating combustion air, is an effective approach that introduced to improve the performance of combustion system. This process is well known as the heat-recirculation combustion or excess enthalpy combustion process (Weinberg, 1971). With this concept, the reactants are highly preheated prior to entering the flame zone and the combustion temperature can be elevated to the super adiabatic temperature compared to the case without heat-recirculation, such as shown in Figure 2.1 (Belmont, 2014). Excess enthalpy combustion has been considered as an effective combustion technology for utilizing a low heating value fuel. However, the main concern with the high combustion temperature is an increase of the thermal nitric oxide formation, leading to increasing NO<sub>x</sub> emission.

In the development of combustion technology, researchers (Tsuji et al., 2003) discovered that an injection of highly preheated combustion air at high velocity into the combustion zone results in combustion with invisible flame and uniformity of the in-furnace thermal distribution. They reported that low O<sub>2</sub> concentration in the flue gas and low NO<sub>x</sub> emission were detected. Thermal efficiency of the combustion system was increased by more than 30% due to recirculation waste heat of flue gas to preheat the combustion air (Tsuji et al., 2003).

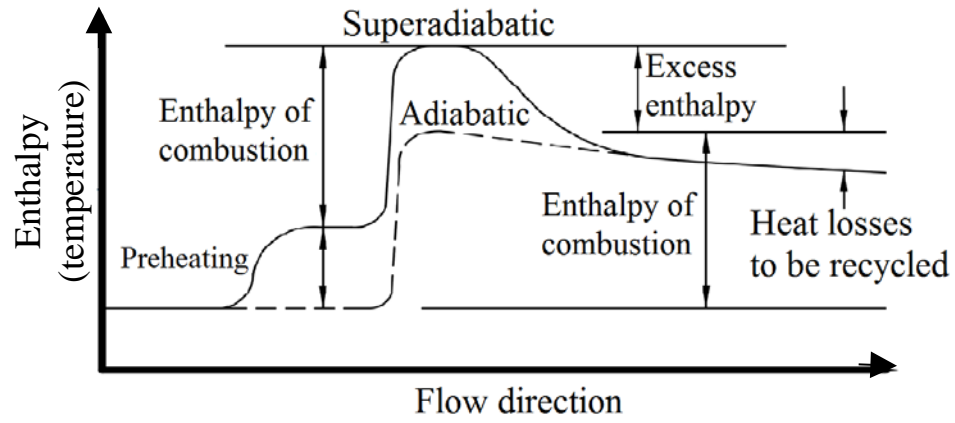


Figure 2.1 Comparison between combustion processes with (solid line) and without (dashed line) heat recirculation (Belmont, 2014)

### 2.1.1 Determination of flameless combustion region

In the practical combustion process, there are different definitions to describe the boundary of flameless combustion based on relationship between temperature and internal gas recirculation rate or dilution level. Wüning and Wüning (1997) proposed that flameless oxidation regime (FLOX) is indicated by the furnace temperature that is higher than auto-ignition temperature ( $T_{ig}$ ) of the fuel and dimensionless recirculation ratio ( $K_V$ ) should be greater than 3 ( $K_V > 3$ ).  $K_V$  is defined as a ratio of exhaust gas recirculation mass flow rate ( $M_E$ ) to the sum of the mass flow rate of combustion air ( $M_A$ ) and fuel ( $M_F$ ):

$$K_V = M_E / (M_A + M_F) \quad (2.1)$$

The other combustion technology development (Tsuji et al., 2003) was carried out based on preheating combustion air, called High-Temperature Air Combustion (HiTAC) which depends on the combustion air temperature and its oxygen

concentration. When oxygen concentration reduces to less than 15% (Gupta et al., 1999) and the combustion air temperature is preheated to higher than  $T_{ig}$ , the combustion process is able to transform into the regime of HiTAC.

Cavaliere and de Joannon (2004) analysed both regimes FLOX and HiTAC and proposed the definition of the combustion regime of Moderate and/or Intense Level of Dilution (MILD), which can be mathematically described as follows: (1) the initial reactant temperature ( $T_{in}$ ) before the combustion must be greater than  $T_{ig}$ ,  $T_{in} > T_{ig}$  while (2) temperature increment during the combustion process ( $\Delta T$ ) is conformed to less than  $T_{ig}$ ,  $\Delta T < T_{ig}$ .

Flameless combustion regime is actually able to occur with the whole range of initial reactant conditions, where the inlet flameless mixture temperature must be sufficiently hot while operating under low reactant dilution levels otherwise a higher dilution level is required (Wang et al., 2014). Rao and Levy, (2010) summarized the definitions of flameless combustion regime into a typical diagram, as shown in Figure 2.2. In this figure, non-premixed strategy flameless combustion is described depending upon hot flue gas recirculation. As recirculation ratio is higher than 0.5, the reactant is diluted into low oxygen concentration of about 12% with inert species of about 88% while preheating reactant temperature higher than the auto-ignition temperature, this region belongs to flameless combustion.



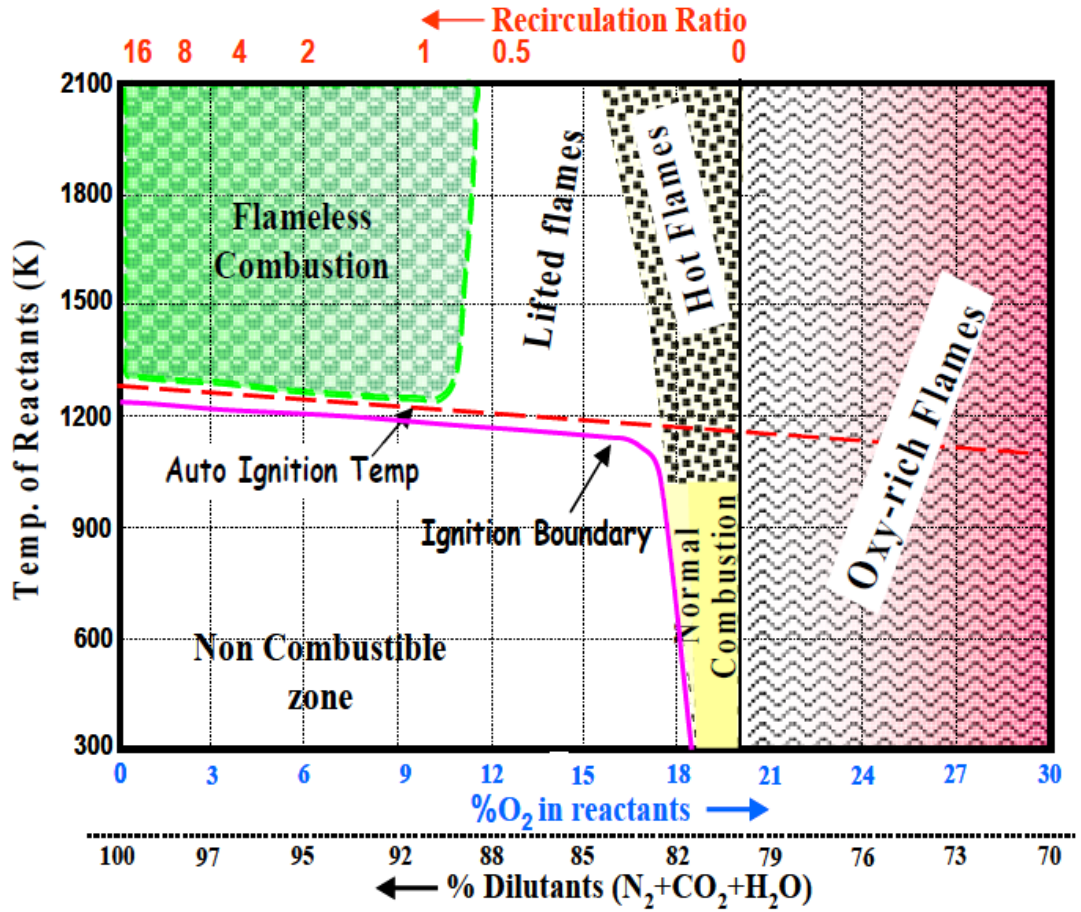


Figure 2.2 Different combustion regimes based on  $O_2$  concentration, recirculation ratio, and reactant temperature (Rao and Levy, 2010)

### 2.1.2 Determination of reaction regime under flameless combustion

Since chemical reaction in flameless combustion is relatively low, its reaction regime can be typified by a slow chemistry regime, depending upon low Damköhler number ( $Da$ ) and high Karlovitz number ( $Ka$ ) ( $Da < 10$  and  $Ka \gg 1$ ) (Jin and Zhou, 2015; Sorrentino et al., 2017). The reaction regime of premixed flameless combustion was examined by Li et al. (2014), which is observed that premixed flameless combustion of methane/air locates in the regime of flamelets-in-eddies typified by moderate  $Da$  and high turbulence characteristics (turbulence Reynolds number -  $Re_t$ ). They also reported that variation of the thermal power load between 7.5 kW and 10

kW did not show a significant effect on the premixed flameless reaction regime. Obviously, equivalence ratio becomes a significant factor that influences the transition of the reaction regime under the flameless combustion process. Khalil and Gupta, (2017) pointed out that decrease of equivalence ratio by increasing Reynolds number in combination with combustion air dilution significantly results in a reaction regime with respect to very low  $Da$ . However, in order to transform a combustion process into the distributed regime,  $Da$  must be reduced in combination with low oxygen where the integral length scale is less than the flame thickness, as shown in Figure 2.3 (Khalil and Gupta, 2017).

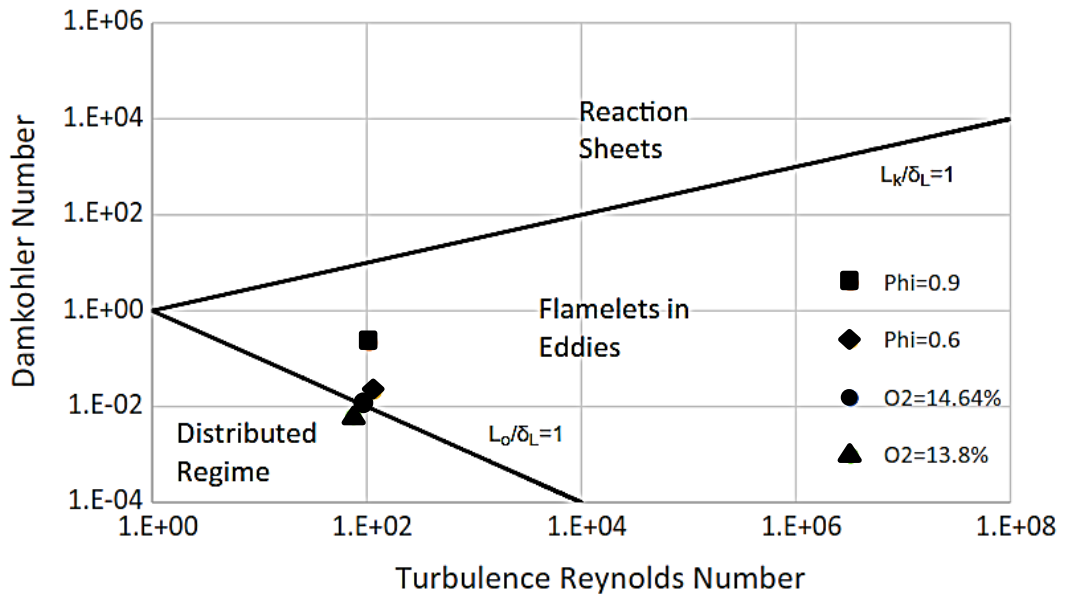


Figure 2.3 Combustion regimes based on Borghi diagram  $Da$  against  $Re_t$  (Khalil and Gupta, 2017):  $L_0$  = integral length scale,  $\delta_L$  = flame thickness, and  $L_k$  = Kolmogorov length scale

In turbulent premixed combustion,  $Da$  is expressed as a ratio of the scale of the characteristic flow time ( $\tau_{flow}$ ) over the characteristic chemical time ( $\tau_{chem}$ ), according to Turns, (2000) as follows:

$$Da = \tau_{flow} / \tau_{chem} \quad (2.2)$$

While  $Ka$  is defined as a ratio of the scale of the characteristic chemical time ( $\tau_{chem}$ ) to the characteristic Kolmogorov time ( $\tau_k$ ), which is a time scale of the small eddy, depending upon the kinematic viscosity ( $\nu$ ) and dissipation ( $\varepsilon$ ) by  $\tau_k = (\nu/\varepsilon)^{1/2}$  (Peters, 1999), as follows:

$$Ka = \tau_{chem} / \tau_k \quad (2.3)$$

## **2.2 Development of PG combustion technology**

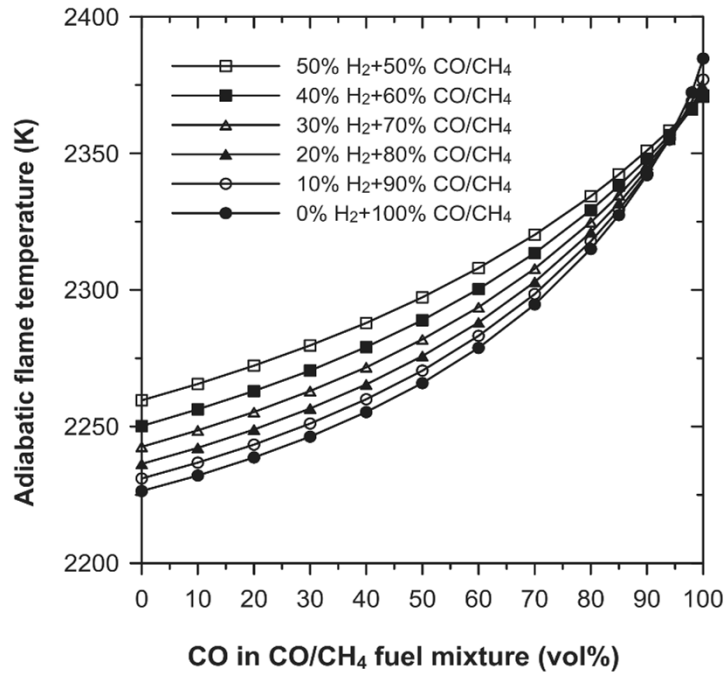
### **2.2.1 PG combustion parameters with burner application**

Although different types of biomass feedstocks can influence the PG composition, the results of combustion parameters such as flame speed, adiabatic flame temperature, wobble index, flame stability, and extinction limits are not significantly varied with the different types of biomass (Hernandez et al., 2008; Lapuerta et al., 2008). This implies that using different biomass materials in a gasification process can be carried out without disturbing the performance of the combustion system. Yan et al. (2010) also implied that with a confined environment combustion, stability of PG flame is not sensitive to compositions of the PG fuel used. In their study, partially premixed burner covered with a conical tube was used to study structures and stabilization of PG combustion. Flame stability has improved significantly when compared to the combustion without the conical tube.

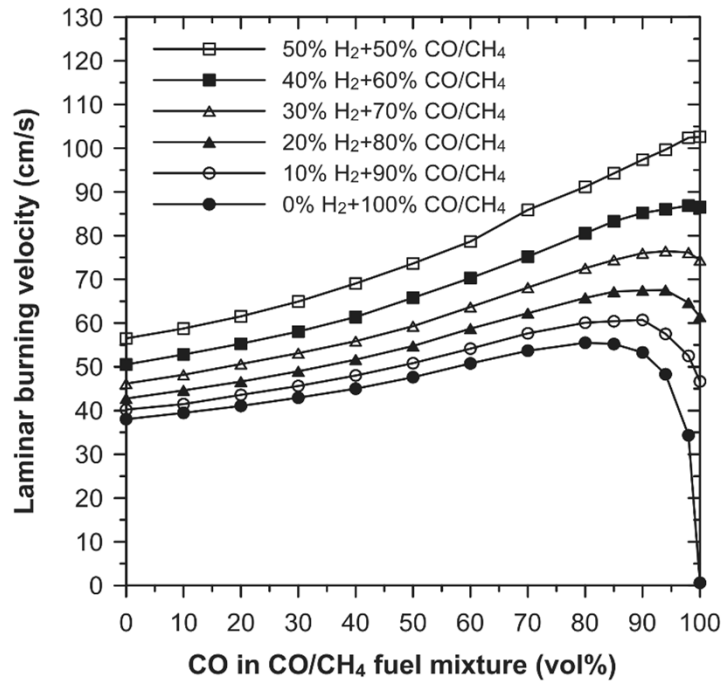
For gas turbine, which designed to operate at low temperature ( $<1200\text{ K}$ ), high quality of gas fuel is not required, but amount of flue gas flow constitutes a significant factor to deliver a full capability of the power generation (Baina et al., 2015a; Rabou et al., 2007). However, combustion of low heating value fuel suffers flame instability and narrow flammability limits (Uchman and Werle, 2016). To improve the flame stability under lean-mixture combustion, mixing PG with natural gas was introduced (Saliamonas et al., 2014) and maximum amount of PG mixed with natural gas should not be higher than 37% (Hernández et al., 2013).

Laminar flame speed and adiabatic flame temperature are two main combustion parameters described the combustion behaviours of low heating value gas fuel (Kalisz et al., 2008). As illustrated in Figure 2.4 (Cheng et al., 2011), both laminar flame speed and adiabatic flame temperature evidently increase with increment of  $\text{H}_2$  and  $\text{CO}$  in a given fuel mixture. However, high  $\text{H}_2$  concentration results in flame instability and flame flashback problems in the combustion process (Kishore et al., 2008; Serrano et al., 2008; Vu et al., 2011).

Liu et al. (2010) studied the flame structures of PGs obtained from different gasification processes. They found that the oxidization layer of these gases is very similar to methane/air flame while their flame thickness has an inverse proportion to the respective laminar flame speed. Furthermore, Munajat et al. (2012) reported that laminar flame speed of PG is sensitive to water vapour ( $\text{H}_2\text{O}$ ) and tar ( $\text{C}_6\text{H}_6$ ) compound in a fuel mixture. A reduction of laminar flame speed was observed with the addition of  $\text{H}_2\text{O}$  into the fuel mixture while the addition of  $\text{C}_6\text{H}_6$  resulted in a non-monotonic trend of laminar flame speed, which initially decreased until reaching a minimum value, and then, increased with an increase of  $\text{C}_6\text{H}_6$ .



(a)



(b)

Figure 2.4 (a) Adiabatic flame temperature and (b) laminar flame speed at stoichiometric mixture of H<sub>2</sub>/CO/CH<sub>4</sub>/air as a function of CO and H<sub>2</sub> additions (Cheng et al., 2011)

Another important parameter related to thermochemical properties of PG combustion is auto-ignition delay. Low combustion temperature and reduced knock tendency of PG are optimal for enhancing the spark ignition engine thermal efficiency without affecting NO emissions (Hernandez et al., 2006). Characterization of PG combustion in a constant volume combustion bomb (CVCB) was investigated by Tinaut et al. (2010) and Soid and Zainal (2014). The results obtained from the CVCB combustion are useful information for determination of operating conditions as well as combustion chamber of internal combustion engine to operate with PG fuel effectively.

Hernandez et al. (2012) characterized the combustion of producer gas obtained from air-blown gasification process through a stability diagram, as shown in Figure 2.5. It can be observed that a stability region covers a lean fuel/air ratio between 0.79 to 1.0 with the maximum reactants velocity of 0.5 m/s to 0.71 m/s and up to 1.18 for a rich mixture with the maximum reactants velocity of about 1.6 m/s. With the confined environment in swirl combustion flow, stable combustion with low CO and NO<sub>x</sub> emissions can be achieved in a range of a lean fuel mixture about 0.49 to the rich fuel of about 1.25 with flue gas temperature between 700 - 1100°C (Al-Attab and Zainal, 2017). Compared to methane, PG combustion is characterized by the shorter auto-ignition delay (Hernandez et al, 2006) and lower both laminar flame speed and adiabatic flame temperature (Ouimette and Seers, 2009). However, laminar flame speed of PG is often greater than that of methane at rich-fuel mixture side and under typical engine operating conditions (Hernandez et al., 2005).

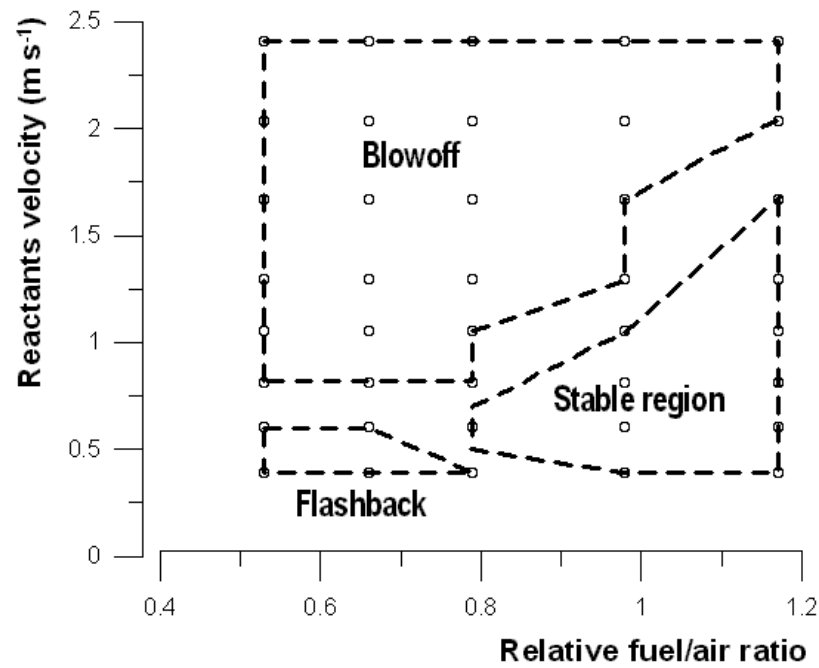


Figure 2.5 Combustion stability diagram for producer gas (Hernandez et al., 2012)

### 2.2.2 Combustion stabilization with swirl vane and bluff-body

A critical concern of PG combustions is unstable flame combustions, which relates to its compositions, low heating value, and local flame temperature as well as mixing fuel/air. A combination of swirl vane and bluff body is a favourable approach to handle this concern. The main idea of this technique is to create high turbulent flow of air and fuel streams in order to achieve good mixing, which will lead to stable reaction of air and fuel and then, enhance the flame stability limits. Flame stabilization using a bluff body and swirl vane for PG combustion is usually applied to the premixed combustion system, as shown in Figure 2.6.

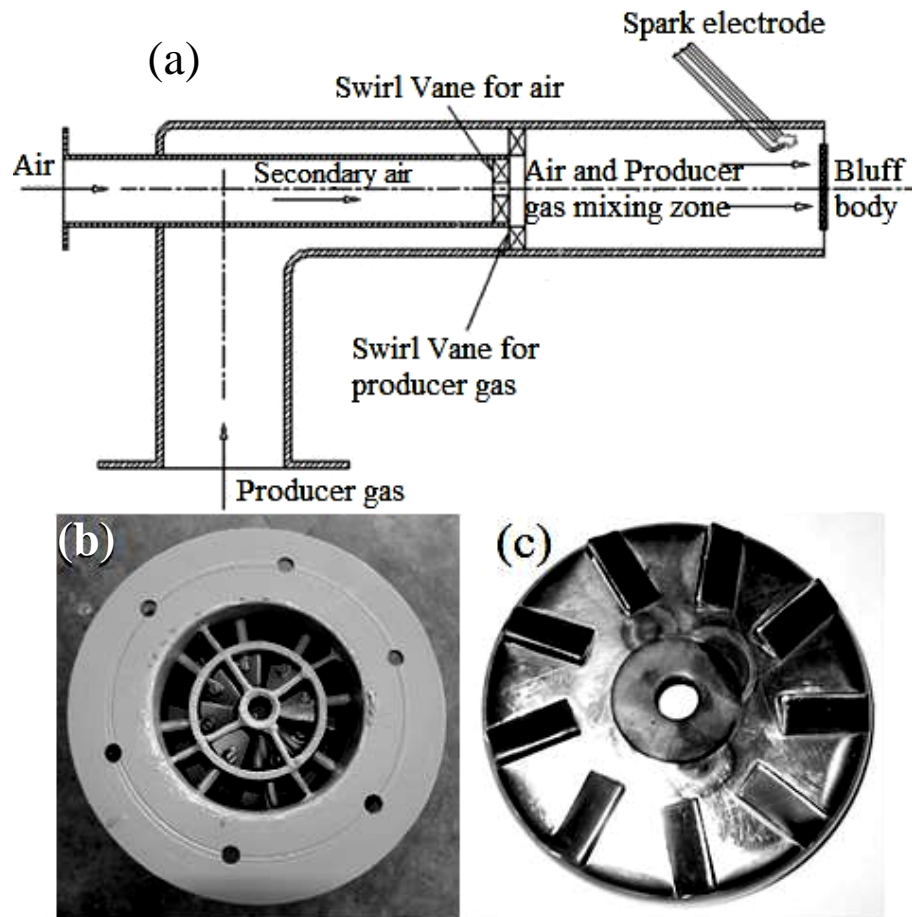


Figure 2.6 (a) Schematic arrangement of burner components (Panwar et al., 2011), (b) swirl vane and (c) bluff body (Bhoi and Channiwala, 2008)

Bhoi and Channiwala (2008, 2009) reported that there are significant effects of a diameter of bluff body and its locations on the flame stability and the peak combustion temperature of PG combustion. The swirl vane used has an optimal angle of the vane of  $60^\circ$ . With this angle, flammability limit is within the range of 40-55%. A bluff body with diameter of 65 mm (corresponding to a blockage ratio of 0.65) located near the nozzle tip is an optimal condition for the nozzle arrangement. At this condition, minimum emission levels of CO and NO<sub>x</sub> were obtained 0.167% and 384 ppm, respectively. The effect of producer gas production on emissions in a swirl vane and bluff body premixed burner was found in an investigation of Panwar et al. (2011). A swirl vane angle of  $60^\circ$  and bluff body diameter of 70 mm, keeping the blockage



ratio of 0.65 were used. They found that both CO and NO<sub>x</sub> emissions decrease with increasing PG flow rate. While the maximum flame temperature is observed at fuel/air ratio of 1.0.

The effect of number of blades in a swirl vane premixed burner on PG combustion characteristics was investigated by Surjosatyo and Priambodho (2011). They found that a swirl vane with 8 blades gives the effective combustion results compared to other swirl vanes with 6 and 10 blades, indicating by minimum CO emissions of 0.02% with maximum temperature of 795°C. While the effect of swirl blade angle on combustion characteristics of PG was investigated by Ilbas and Karyeyen (2017), which reported that the flame temperature increases as the swirl blade angle increases. CO<sub>2</sub> distribution is increased whereas CO decreases in the flame zone with increasing the swirl blade angle. Punnarapong et al. (2017) modified an existing liquefied petroleum gas (LPG) burner into a premixed PG burner for utilizing in a furnace of ceramic manufacturing industry. The modified PG burner is able to operate well at thermal power input within the range of 30-40 kW with maximum flame temperature of 1200°C. Thermal efficiency is in the range of 84-91% and acceptable range of CO and NO<sub>x</sub> emissions are observed.

Ge et al. (2016) used a double-swirled burner to study effect of H<sub>2</sub>O on non-premixed combustion characteristics and flame structure of PG. They reported that an increase of H<sub>2</sub>O in combustion air results in decreasing concentration of OH radicals, leading to a reduction of the main reaction zone and the average exhaust temperature, which is the main result of decreasing NO formation. Moreover, the humidity can also reduce the lift-off flame of PG combustion. Air humidification level within low (<25%) to medium (25%) is considered as the optimal condition. With a higher air

humidification (>25%) increases N<sub>2</sub> dilution and also results in increasing CO and NO<sub>x</sub> emissions (Tian et al., 2016).

### **2.2.3 PG combustion in staged combustor**

A staged combustion chamber with axial and radial reactants injections was used as a combustor for operating a single shaft micro-gas turbine using dual-fuel mode of PG and LPG (Sadig et al., 2015). The combustor performance was examined in terms of LPG fuel replacement and emission characteristics. The study reported that radial air injection gives a higher LPG replacement ratio than that of axial air injection. When LPG is replaced with producer gas, NO<sub>x</sub> emission decreases but CO emission increases for both injection methods. Mandl et al. (2011) designed an air staged combustion chamber, which separated a fuel-rich zone from an oxidizing zone in order to prevent NO-formation and to burn the remaining fuel in a flue gas mixture. The results showed that complete PG combustion is achieved.

NO<sub>x</sub> emission from PG combustion is sensitive to the nitrogen content in the biomass feedstock. This is pointed out by researchers (Sethuraman, 2010; Sethuraman et al., 2011; Van Huynh and Kong, 2013). They reported that thermal NO<sub>x</sub> is significantly less than fuel-NO<sub>x</sub> constituted as a majority of the total NO<sub>x</sub> emissions. Besides, NO<sub>x</sub> emission does not noticeably change with varying combustion equivalence ratio, but it significantly increases with increment of the combustion heat load. Based on the numerical simulations, Sukumaran and Kong (2013) suggested that fuel NO<sub>x</sub> formation can be reduced by designing combustion conditions and using a bluff body. This method will allow the major NO<sub>x</sub> generation to pass over the fuel rich